Time-dependent seismic fragility curves for post-tensioned timber frames

Gabriele Granello[a], Marco Broccardo[b], Alessandro Palermo[c] and Stefano Pampanin[d]

Since 2010, a significant worldwide increment in the construction of post-tensioned timber (Pres-Lam) buildings has been observed. Pres-Lam technology combines unbonded post-tensioning tendons and supplemental damping devices to provide moment capacity to beam-column, wall-foundation or column-foundation connections. In low seismic areas, designers may choose not to provide additional damping, relying only on the post-tensioning contribution. Because post-tensioning decreases over time due to creep phenomena arising in compressed timber members, a reduction of the clamping forces between the elements occurs. This reduction affects the seismic response of PresLam buildings in the case of low and high intensity earthquakes. A possible method to evaluate the seismic performance of post-tensioned timber frame buildings, through the computation of time-dependent fragility curves, is presented in this paper. The method is applied to two case studies, designed respectively with and without supplemental damping devices. In terms of structural performance, results show that the use of additional dissipaters mitigate the effect of post-tensioning loss for earthquakes of high intensity. Conversely, performance under low intensity earthquakes is strongly dependent on the post-tensioning value, as the reduction of stiffness due to the anticipated rocking motion activation would lead to damage to non-structural elements.

INTRODUCTION

During the 1990s, the Precast Seismic Structural System (PRESSS) program (Priestley, 1991) coordinated by the University of California, San Diego, proved that the hybrid connection is an efficient low-damage solution for precast concrete walls and frames. The hybrid connection combines unbonded post-tensioning tendons and additional dissipation devices or internal

[a]Lecturer, Department of Civil Engineering, University of Canterbury, New Zealand
[b]Post doctoral fellow, Department of Civil Engineering, ETH Zurich, Zurich.
[c]Professor, Department of Civil Engineering, University of Canterbury, New Zealand
[d]Professor, Department of Civil Engineering, University of Canterbury, New Zealand

reinforcement, allowing the accommodation of the seismic demand through rocking between structural elements.

Unbonded tendons provide re-centering capabilities to the building, while dissipation devices allows for hysteretic energy release as well as providing additional moment capacity. These damping devices can be placed internally, by de-bonding mild steel reinforcement bars, (e.g., (Curtain et al., 2012)), or externally, (e.g., (Marriott et al., 2009; Sarti et al., 2016)), to the connection. However, when they are externally placed, they have the additional advantage of being easily accessible for replacement.

In 2002, Christopoulos et al. (2002) extended the hybrid concept to steel members . This fact supports the idea that the hybrid connection is materially independent. In 2005, at the University of Canterbury (Palermo et al., 2005) the technology was extended to engineered timber products and was referred to as the Pres-Lam system.

Extensive laboratory testing in New Zealand (Newcombe et al., 2008; Sarti et al., 2015; Moroder et al., 2018) and overseas (Wanninger and Frangi, 2014; Kramer et al., 2015; Di Cesare et al., 2017; Li et al., 2018) has proven the hybrid connection to have good seismic performance, which was characterized by no residual displacements, negligible structural damage in the timber members, and stable non-degrading hysteretic response. In the subsequent years, the Pres-Lam system was applied as a structural system for several timber buildings erected in New Zealand (Curtain et al., 2012; Brown et al., 2012; Holden et al., 2016) and overseas (Leyder et al., 2015; Sarti et al., 2017b).

Few experimental campaigns, in terms of long-term performance (Davies and Fragiacomo, 2011; Wanninger et al., 2014; Granello et al., 2017), were conducted aiming to quantify post-tensioning losses in post-tensioned timber structures. These studies outlined that the most relevant quantities governing the post-tension loss phenomenon were the amount of timber loaded perpendicular to the grain, and environmental conditions. In fact, when timber is loaded perpendicular to the grain higher creep is expected (Morlier, 2004), and therefore also higher post-tensioning loss. A design procedure to assess the amount of post-tensioning loss was also developed (Granello et al., 2018), which provided reasonably good results when compared to the average experimental data monitored on operative buildings within the observation period. However, the variability within the material behavior increases the uncertainty in the post-tensioning prediction. Specifically, a greater uncertainty is expected when results are extrapolated outside the observation time frame over the life of the structure..

Figure 1. Examples of operative PresLam structures and beam-column joint detailing: a) Trimble Navigation Offices, Christchurch (courtesy of Paul Drummond) using b) external steel plates in the beam column joint; c) ETH House of Natural Resources, Zurich (copyright ETH Zurich-Marco Carocari) using d) hardwood columns (copyright ETH Zurich-Marco Carocari); e) Merritt Building, Christchurch (courtesy of Andy Buchanan) using f) internal steel plates (courtesy of Andy Buchanan).

This paper provides a method to estimate the time-dependent seismic performance of PresLam frame buildings. The seismic performance is evaluated by developing fragility curves, whose parameters are time-dependent. The uncertainty due to ground motions variability, as well as the uncertainty due to the development of post-tensioning losses, is in taken into account. The method is applied to two case studies. In Case Study 1, the structure is placed in high seismic area, and designed by providing additional dissipation devices. In Case Study 2, the structure is designed in low seismic area and relies only on post-tensioning contribution to provide a moment resisting connection between beams and columns. It is conceivable that in low seismic risk areas that a designer may choose not to include external dissipaters.

CASE STUDY BUILDINGS

DESIGN

Two case study buildings are designed to be placed in a low (i.e. corresponding to maximum spectral acceleration in correspondence of the plateau equal to 0.54 g for a 500 years return event) and high (i.e. corresponding to a maximum spectral acceleration in correspondence of the plateau equal to 0.9 g for a 500 years return event) seismic risk area, respectively. While the first building is only post-tensioned, the second one is designed with dissipation devices at the beam-column rocking interface. Both structures are designed to be located on type D soil (New Zealand Standard 1170.5, 2004), corresponding to a deep or soft soil site. The buildings proposed are a further development of the case study specimen (Figure 2) presented in the New Zealand and Australian Guideline for post-tensioned timber buildings (Pampanin et al., 2013). The structural systems used in that specific case-study were Pres-Lam frames in the transverse direction and Pres-Lam walls in the longitudinal direction. This paper focuses on the seismic behavior of the frames, which are re-designed to serve as a design case study for this work.

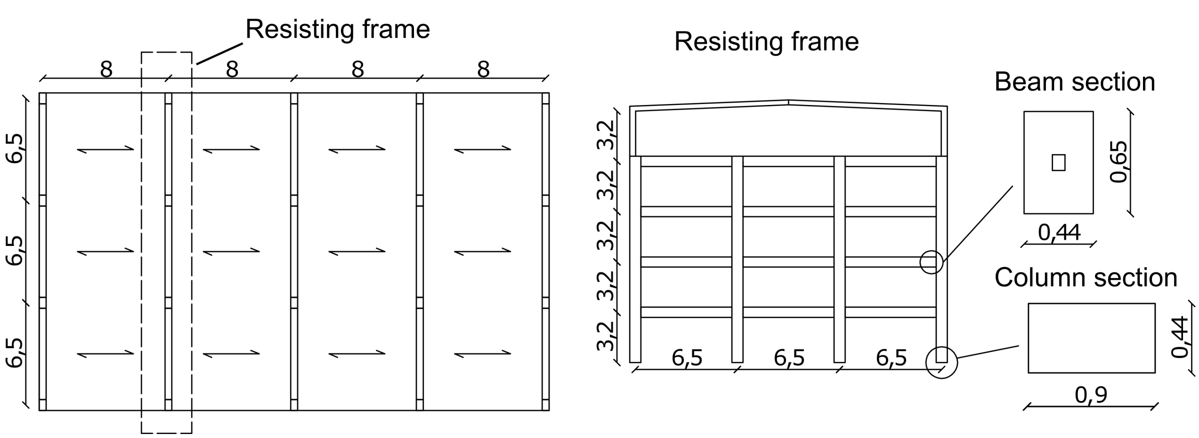

Figure 2. Plan view of the floor, lateral view of the frame and members' section (note units are in meters).

The two four-storey case study buildings are designed with a lightweight timber penthouse at the top floor. Each floor is selected to be 32 x 19.5 m in plan with a total floor area of 624 square meters (Figure 2). A building live load of 3 kPa (i.e. office use according to the New Zealand Standard (1993)) is assumed to act on a floor system made up of 21 mm thick plywood panels on top of 90 x 400 mm timber joists at 0.6 m. To be consistent with the design assumptions reported in the guidelines, no concrete is placed on the top (Pampanin et al., 2013). The design is carried out by using a displacement-based approach (Priestley et al., 2007). However, the members size and post-tensioning value are governed by the deflection limits to not be exceeded during low intensity seismic events or excessively strong winds. According to the New Zealand Standard 1170.1 (1993) , an interstorey drift equal to 0.33% should not be exceeded for an event with a return period equal to 25 years. Therefore, beam and column dimensions of 650 x 441 mm, and 900 x 441 mm respectively, are required to meet these criteria. The timber material used for the design is LVL grade 16, properties which according to the manufacturer are reported in Table 1. For the building placed in low seismic hazard, cross sections with lower dimensions could be designed to optimize the material use. However, in order to compare the results between the two cases, it has been decided to keep the same elements' size.

Table 1. LVL Grade 16 properties: f_b bending strength, $f_{c,par}$ compression strength parallel to the grain, $f_{c,perp}$ compression strength perpendicular to the grain, f_s shear strength, E_{par} elastic modulus parallel to the grain, E_{perp} elastic modulus perpendicular to the grain, G shear modulus.

f_b (MPa)	$f_{c,par}$ (MPa)	$f_{c,perp}$ (MPa)	f_s (MPa)	E_{par} (MPa)	E_{perp} (MPa)	G (MPa)
65	48	12	4.6	16	0.55	0.8

A summary of the seismic masses (considering the proper combination of dead and live loads according to the New Zealand Standard 1170.5 (2004)) is reported in Table 2.

The beam-column connection (detailed in Figure 3) with the addition of the external dissipation devices (Sarti et al., 2016), is designed to target a design re-centring ratio at the Ultmate Limit State (ULS), β_{rec}, (defined as the ratio between the post-tensioning moment contribution over the total moment capacity) of 0.7. Seven wire strands (properties reported in Table 3) are used as the post-tensioning elements. However, the number of tendons is optimized at each for the two buildings according to the layout reported in Table 4. Ten millmetre external steel plates are designed (see Figure 3 and Figure 2b) to protect the timber in the column, which is

Table 2. Seismic masses acting on the frame.

Floor	Mass (KN)	Mass (KN/frame)	Mass (KN/wall)
4	3130	626	782
3	3193	639	798
2	3193	639	798
1	3193	639	798
Tot	12710	2542	2542

loaded perpendicular to the grain. This solution, which was adopted in the Trimble Navigation Offices (Brown et al., 2012), also showed to have a beneficial effect in reducing the amount of post-tensioning loss expected (Granello et al., 2018), as well as providing an anchorage point for the dissipaters.

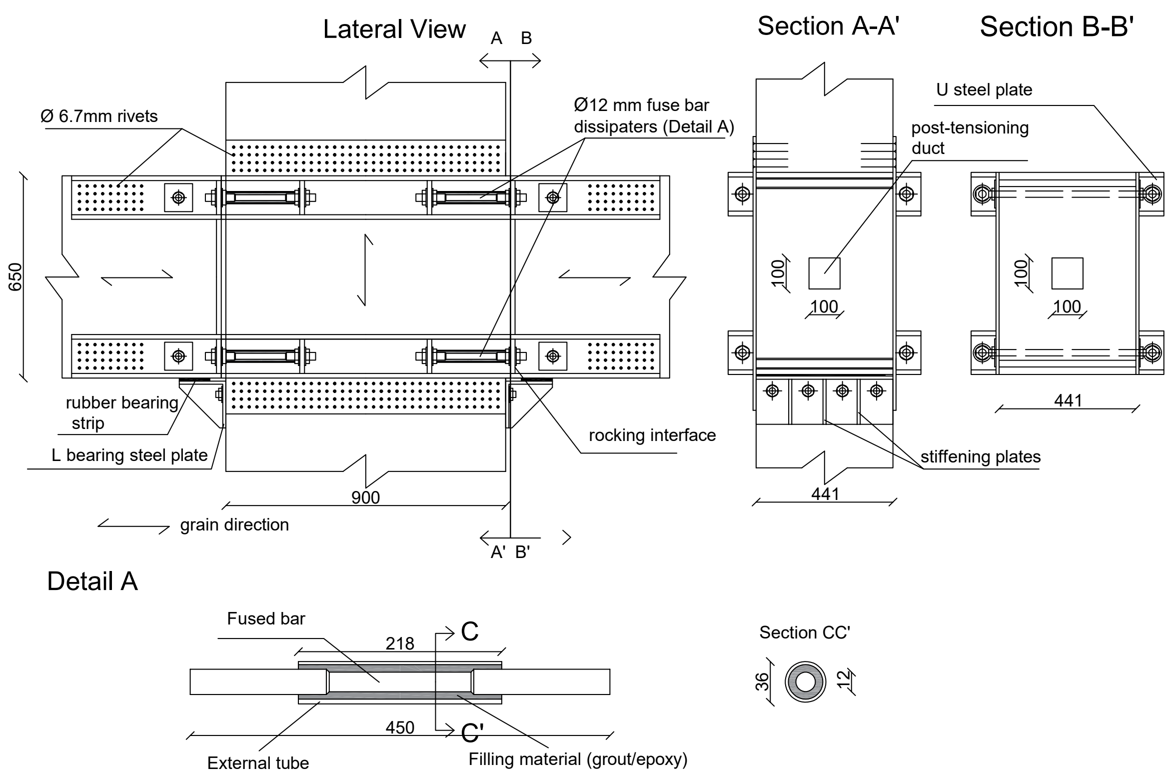

Figure 3. Structural detailing: beam-column hybrid joint and fuse dissipater.

While post-tensioning tendons are positioned at the section centroid of the beam section, dissipaters are placed ± 250 mm from the beam centreline (see Figure 3). The properties of the mild steel, used to fabricate the dissipaters, are reported in Table 5, while the dissipaters layout

Table 3. Steel tendon properties: Φ_i tendon diameter, A_{pi} tendon area, f_{ptk} ultimate stress, f_{pt01k} nominal yielding stress and E_p elastic modulus.

Φ_i (mm)	A_{pi} (mm^2)	f_{ptk} (MPa)	f_{pt01k} (MPa)	E_p (GPa)
12.7	100.1	1860	1674	195

Table 4. Post-tensioned connection detailing with and without additional damping.

	Storey	**Tendons number**	**Post-tensioning force (KN)**	**Tendons stress (% f_{pt01k})**	**Mild steel dissipaters**
With Dissipaters	1&2	3	300	60%	4Φ12
	3&4	2	200	60%	4Φ10
Without Dissipaters	1&2	2	200	60%	-
	3&4	2	200	60%	-

is reported in Table 4.

The differences between the two case study buildings are not limited to the use of dissipaters in one of the two. Specifically, a moment resisting connection (detailed in Figure 4) is designed at the column-foundation level, by introducing internal 14 mm diameter steel bars, for the building placed in high seismic area. This detailing was necessary to increase the stiffness of the frame, and therefore limiting the interstorey drift within an acceptable value for low intensity earthquakes. The connection between timber and steel was obtained by injecting epoxy, and the bars were de-bonded for a total length of 200 mm to distribute the plastic demand. A similar solution with the internal bars was previously adopted for the Carterton Event Centre (Curtain et al., 2012).

The possibility of introducing external dissipaters, which would be easier to replace, was also explored. However, this solution was not feasible due to the high number of connectors necessary between the dissipaters and the column. Shear keys are also provided for transferring shear and avoiding the internal bars working in dowel action.

Table 5. Mild steel properties respectively: f_y yielding stress, f_u ultimate stress, E_s elastic modulus, ϵ_y yielding strain, r post-yielding stiffness ration.

f_y (MPa)	f_u (MPa)	E_s (MPa)	ϵ_y $(-)$	r $(-)$
300	420	200	0.0015	0.008

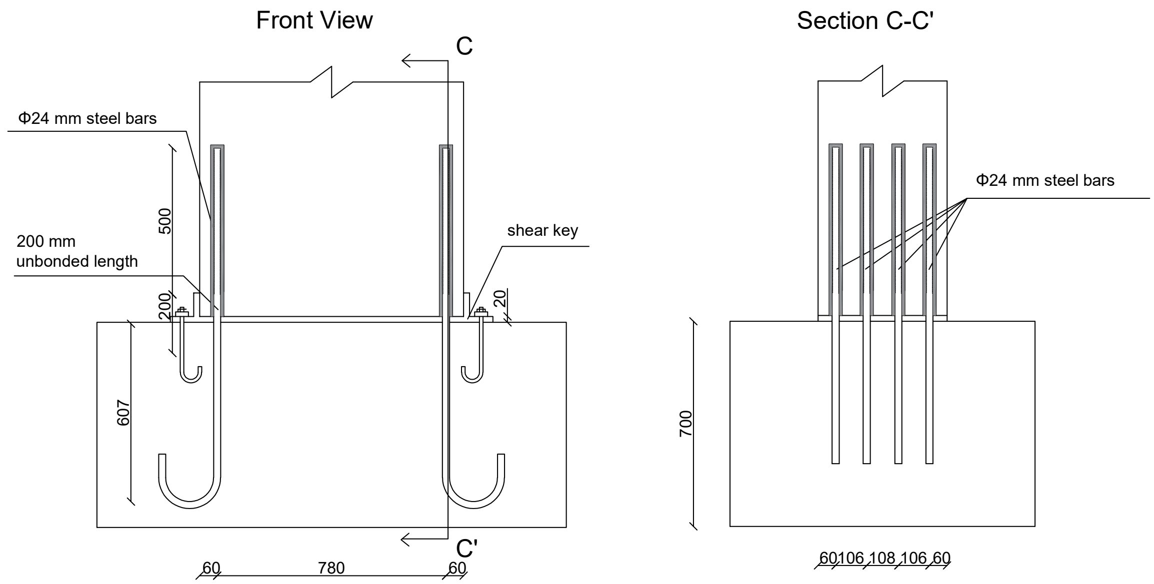

Figure 4. Column-to-foundation structural detailing.

MODELLING APPROACH

The moment-rotation behavior of a post-tensioned rocking connection was defined using an iterative analytical procedure developed by Pampanin et al. (2001), modified by Palermo et al. (2004), and extended to the Pres-lam system by Newcombe et al. (2008), and further developed by Smith (2014). Such moment-rotation laws are implemented in the literature on lumped plasticity models, using multi-spring elements (Sarti et al., 2017a), or rotational spring elements (Ponzo et al., 2017). The difference between the two is the ability of the multi-spring model to capture the increase of axial force in the system due to the beam elongation phenomenon. Given the large inertia of the member, this phenomenon is rather important when looking experimentally at the behaviour of post-tensioned walls (Sarti et al., 2015). However, in the case of post-tensioned frames models based on rotational springs were shown to adequately (up to acceptable errors) predict the behavior of post-tensioned timber specimens when compared to the shaking table test (Di Cesare et al., 2017).

In this work, lumped plasticity models (see Figure 5) were then calibrated against the moment-rotation response using rotational springs in parallel and in series as follows: (i) a multi-linear elastic hysteresis for the post-tensioning contribution, (ii) an elasto-plastic rule for the mild steel contribution, and (iii) an elastic-rigid rule for the internal rotation before the gap opening contribution. An additional rotational spring was placed at the beam-column joint to take into account the joint shear stiffness, as recommended by Smith (2014). Besides the joints (including the column-to-foundations one), all the other elements are modeled as elastic members.

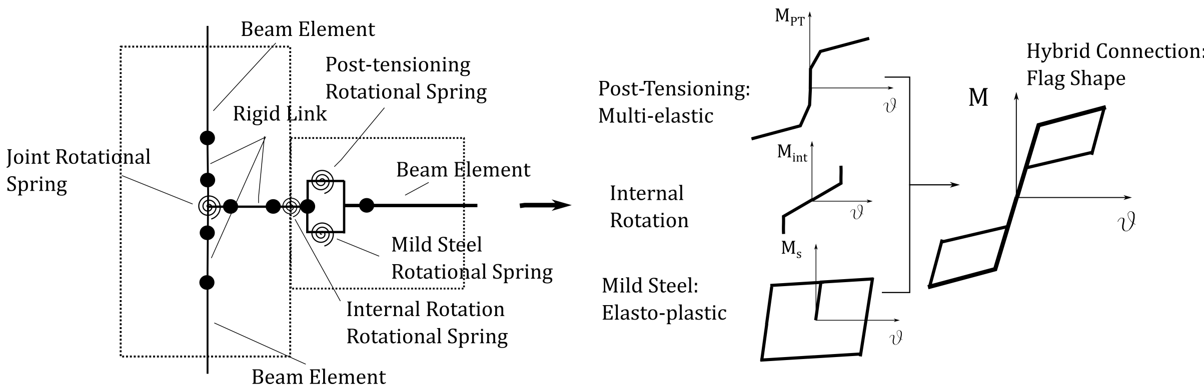

Figure 5. Post-tensioned timber connection modelling.

POST-TENSIONING LOSS ESTIMATION

A design procedure for estimating post-tensioning losses in post-tensioned timber frames was developed by Granello et al. (2018). According to such procedure, the post-tensioning loss over time $\Delta P(t)$ was estimated according to Equation 1:

$$-\Delta P(t) = \frac{-P_0\left\{\frac{l_{\|}\phi_{\|}(t)}{E_{\|}A_{\|}} + \frac{l_{\perp}\phi_{\perp}(t)}{E_{\perp}A_{\perp}} + \frac{lr_p(t)}{E_pA_p[1-\chi(t)_p r_p(t)]}\right\} + \Delta\epsilon_{\|,in}(t)l_{\|} + \Delta\epsilon_{\perp,in}(t)l_{\perp} - \Delta\epsilon_{p,in}(t)l}{\frac{l_{\|}[1+\chi(t)_{\|}\phi_{\|}(t)]}{E_{\|}A_{\|}} + \frac{l_{\perp}[1+\chi(t)_{\perp}\phi_{\perp}(t)]}{E_{\perp}A_{\perp}} + \frac{l}{E_pA_p[1-\chi(t)_p r_p(t)]}} \tag{1}$$

where the indices $_{\|,\perp}$ refer to the correspondent timber properties parallel and perpendicular to the grain, respectively. The index $_p$ instead refers to the post-tensioning steel properties; l, A, E respectively represent the length of timber under load, the cross-sectional area and the elastic modulus; $\phi(t), r_p(t)$ represent the timber creep function and the steel relaxation function. The terms $\Delta\epsilon_{in}$ represent the inelastic deformation due to changes in environmental conditions and P_0 the initial post-tensioning force. The function $\chi(t)$ takes into account that the analytical solution is approximated by correcting the creep or relaxation function Chiorino et al. (1984). The reader specifically interested in the post-tensioning loss calculation is redirected to (Granello et al., 2018) for a comprehensive overview.

It is assumed that the timber elements are delivered on site with an average moisture content equal to 12%, and that the environmental temperature at the time of pre-stressing is equal to $10°C$. The predicted post-tensioning trend over time, $\mu_{PT}(t)$, is reported in Figure 6 and Table 6. It can be noticed that the mean predicted value in 50 years is equal to 16%. The reason for such a 'limited' amount, among other factors such as the use of steel plates in the beam-column joint, is because the ratio between the post-tensioning steel area A_p over the timber section $A_{\|} = A_{\perp}$ is very low . When the procedure was used to evaluate the amount of post-tensioning loss of the Trimble building (Granello et al., 2018), it provided reasonable results considering the average value of the load cells. However, if the prediction is compared with each single load cell, it is subjected to greater uncertainty due to the intrinsic variability of each frame. Figure 7 shows the empirical standard deviation of the error (STD) between the prediction and each load cell for the Trimble Navigation Offices. It can be observed that the uncertainty on post-tensioning loss is increasing with time. To capture this trend, a power law is selected to model the STD, i.e .

$$\sigma_{PT}(t) = c_1 t^{c_2}, \tag{2}$$

where c_1, c_2 are parameters of the model. Figure 7 shows the selected model together with the original data. Equation (2) captures fairly well the time evolution of the empirical STD. The post-tensioning force, PT[a], can be expressed as

$$PT_t = \mu_{PT}(t) + \varepsilon_t, \tag{3}$$

where $\varepsilon_t \sim \mathcal{N}(0, \sigma_{PT}(t))$, are zero mean Gaussian random variables with standard deviation defined at a given time t by Equation (2). The subscript $\cdot_t$ is used to indicate the time dependence of the process, i.e. at a given time t, PT_t is a Gaussian Random variable with mean $\mu_{PT}(t)$ and STD $\sigma_{PT}(t)$. It is considered out of the scope of the current study to complete a second order description of the process (e.g., by defining an autocorrelation function).

In addition to the average losses, Figure 6 and Table 6 report the average value plus (PT^{+}_{2STD}) and minus (PT^{-}_{2STD}) to be two times the standard deviation. Therefore, the green area in Figure 6 represents the possible post-tensioning scenarios within a confidence of 95%, and the average value is represented by the dotted black curve. Note that the initial value is not 100% because of the inelastic deformation of timber and steel at the moment of stressing, which are assumed

[a] Capital letters for PT are used only to indicate the variable "Post Tension," and not to identify a random variable. Therefore PT is deterministic. Conversely, the authors define PT_t as proper random variable defined at time t by Equation (3).

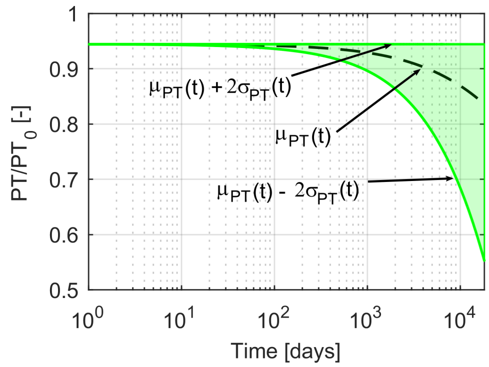

Figure 6. Post-tensioning force over time according to (Granello et al., 2018). $\mu_{PT}(t)$ average value, $\mu_{PT}(t) + 2\sigma_{PT}(t)$ upper bound and $\mu_{PT}(t) - 2\sigma_{PT}(t)$ lower bound.

Table 6. Post-tensioning force evolution over time: $PT_{avg} = \mu_{PT}(t)$ average value, $PT^{-}_{2STD} = \mu_{PT}(t) + 2\sigma_{PT}(t)$ upper bound and $PT^{-}_{2STD} = \mu_{PT}(t) - 2\sigma_{PT}(t)$ lower bound.

Post-tensioning	Intial	10 years	25 years	50 years
PT_{avg}	100%	91%	87%	84%
PT^{+}_{2STD}	100%	94%	94%	94%
PT^{-}_{2STD}	100%	82%	70%	55%

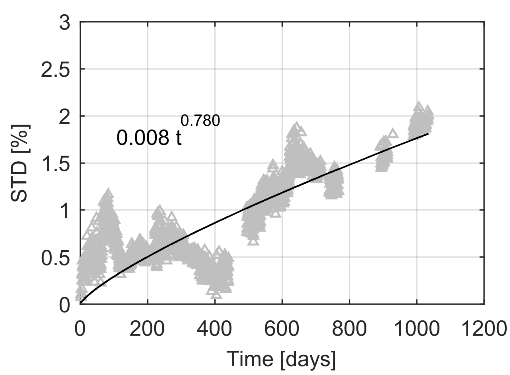

Figure 7. Standard deviation of the error (STD) between the prediction and the data monitored in the Trimble Navigation Offices (Granello et al., 2018).

to occur instantaneously. This value is also considered as the upper boundary of the prediction, which implies a truncated Gaussian distribution for ε_t.

QUANTIFICATION OF THE PERFORMANCE

INDICATORS AND PERFORMANCE LEVELS

The quantification of the building's performance is carried out by looking at specific indicators similar to FEMA P650 (2009). In this study, two sets of indicators are proposed:

1. performance levels in terms of materials strain limit;
2. performance levels in terms of interstorey drift;

Performance levels in terms of materials strain limits

Within this set, performance levels are defined at material level i.e., as the limits in terms of stress or strain which affect the behavior of the system. The main idea of the PresLam system, and in general of controlled rocking connections, is to dissipate the energy within the connections leaving undamaged the main structural elements. According to this principle, the following performance levels are defined when considering the rocking connection behavior:

- $PL1_{y,ms}$: dissipaters yielding (if present);
- $PL2_{u,ms}$: dissipaters rupture (i.e. assumed occurring at 6% axial deformation according to Priestley (2000));
- $PL3_{y,t}$: timber yielding;
- $PL4_{y,p}$: tendons yielding;
- $PL5_{u,p}$: tendons rupture;

$PL1_{y,ms}$ and $PL2_{u,ms}$ can be classified as serviceability damage state (SLS) because the dissipaters have to be replaced at the end of the seismic event. Conversely, $PL3_{u,t}$ and $PL4_{y,p}$ can be considered as ultimate limit states (ULS) because the structural members are permanently damaged or major repairs are necessary. Finally, $PL5_{u,p}$ is considered as collapse limit state because the system fails.

In Figure 8 it is reported the moment-rotation response of the beam-column joint of the specimen with dissipaters. Specifically, the response refers to the joints at the first storey. The

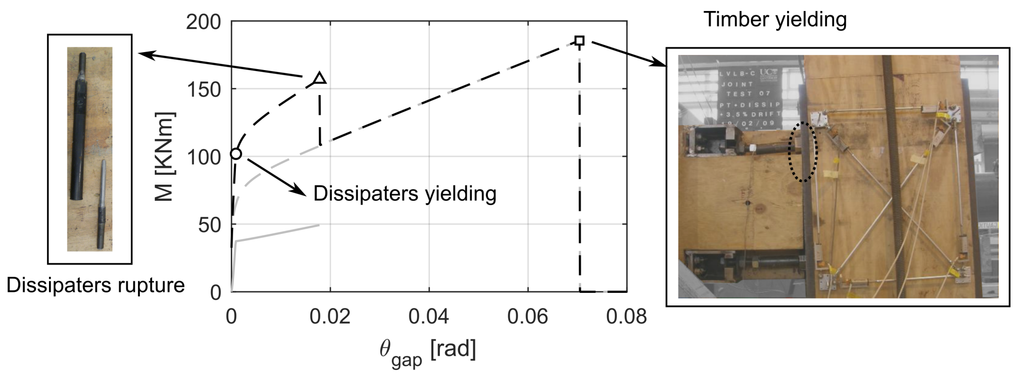

Figure 8. Performance levels for the hybrid rocking connection on the moment-rotation response.

performance levels are also highlighted. It can be noticed that $PL1_{y,ms}$ occurs almost immediately after the decompression of the joint, for a $\Theta_{gap} = 0.001$. Once the rocking motion is triggered, the dissipaters are activated soon after subjected to yielding.

The dissipaters rupture, i.e., $PL2_{u,ms}$, occurs for approximately $\Theta_{gap} = 0.02$; this value can be controlled during the design phase by modifying the unbonded length of the dissipaters. The current practice (Pampanin et al., 2013) suggests designing dissipaters by having an axial deformation equal to 3% at the ULS, which normally targets a 2.5% drift. The building is designed by following this recommendation, therefore, a gap opening equal to $\Theta_{gap} = 0.02$ occurs after reaching 2.5% drift. Once the dissipaters break, their contribution in terms of moment is set equal to 0.

The timber yielding $PL3_{y,t}$, meaning that the most compressed timber fibers exceed the yielding deformation, occurs at approximately $\Theta_{gap} = 0.07$. In this case, the performance level is reached in the beam because the column is protected by steel plates. However, if the column is not adequately protected by using hardwood or steel, this performance level can be reached at lower rotations as the strength of timber perpendicular to the grain is significantly lower than the strength of timber parallel to the grain.

When timber locally yields, the inertia of the entire section is reduced causing a degradation of stiffness. This would imply great rotations, and therefore more fibers would be progressively subjected to yielding. A more refined model, using a more detailed approach, should be used to capture this progressive degradation (Valipour et al., 2016). However, it is conservatively assumed that the moment being carried by the connection, after the yielding of timber, is equal to 0.

The moment-rotation analysis was stopped at $\Theta_{gap} = 0.08$. In fact, given this gap opening the building would have an interstorey drift $\Theta_{interstorey}$ greater than 8%. This happens because $\Theta_{interstorey}$ is the sum of gap opening Θ_{gap} and elastic deformation Θ_{el}:

$$\Theta_{interstorey} = \Theta_{el} + \Theta_{gap} \tag{4}$$

Although the New Zealand building code does not specify a drift limitation in terms of collapse limit state, a limit should be introduced to verify the structure against Maximum Credible Earthquakes (MCE) (Hare et al., 2012). In this study, 6% interstorey drift is considered as the collapse limit state.

Because of this assumption, the local performance of the connection has a lack of meaning after 6% interstorey drift. Within this limit, the yielding, or even rupture, of tendons is not occurring. Analyses conducted for different connections have shown that the yielding of tendons always occur at very large interstorey drift (greater than 6%). This is due to timber flexibility: because of the great elastic deformation Θ_{el}, the maximum allowable gap opening Θ_{gap} is limited for a given $\Theta_{interstorey}$.

Performance levels in terms of interstorey drift

Within this set, performance levels are defined in terms of interstorey drift. Although its values are conventional, they are used as indicators in several building codes, e.g. New Zealand Standard (2004), FEMA P650 (2009) and Eurocode 8 (2005). The following values were considered:

- $PL1_{dr}$: interstorey drift greater than 0.33%. Exceeding this value would cause damage to no-structural elements (Figure 9a) as suggested by the New Zealand Standard 1170.0 (2002), Appendix C.
- $PL2_{dr}$: interstorey equal to 2.5%. This value represented the ultimate limit state or controlled damage (Figure 9b) as proposed by New Zealand Standard 1170.5 2004, Section 7.5.1.
- $PL3_{dr}$: interstorey equal to 6%, assumed as collapse limit state (Figure 9c).
- $PL4_{dr}$: residual interstorey drift greater than 0.5%. If this value is exceeded, the reoccupancy of the building is not possible (Figure 9d). The building is likely to be demolished due to uneconomical repairs (McCormick et al., 2008; Hare et al., 2012).

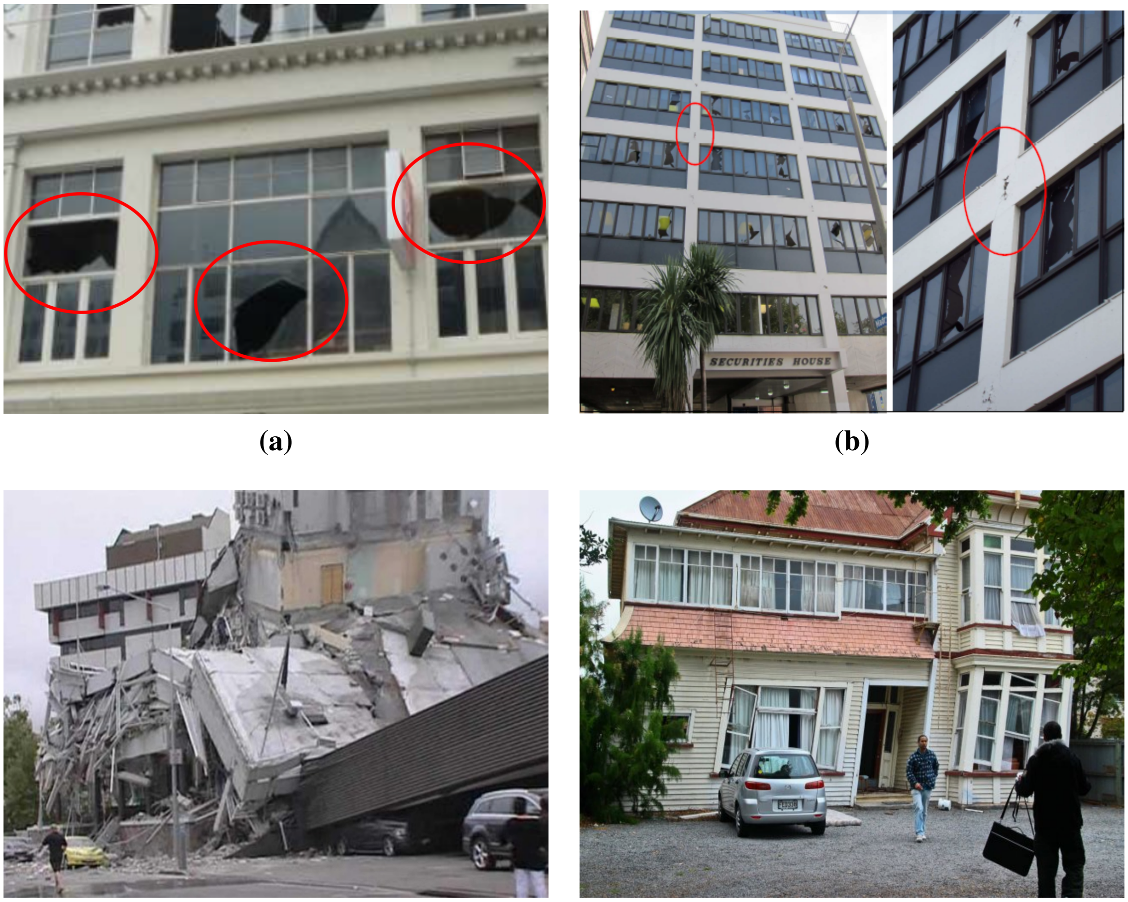

(a) (b)

(c) (d)

Figure 9. Performance levels: A) $PL1_{dr}$, expected damage to no structural elements (courtesy of Stefano Pampanin) ; B) $PL2_{dr}$, expected damage to structural elements (courtesy of Stefano Pampanin) C) $PL3_{dr}$, expected significant damage or collapse (source: www.tvnz.co.nz); D) $PL4_{dr}$, expected residual deformation after the seismic event (photo taken by Asher Trafford, source https://keithwoodford.wordpress.com/2011/02/27/understanding-the-christchurch-earthquake-building-damage).

Combined performance levels

The performance levels described above are combined to have a unique set:

1. $PL_{1,a}$ defined as serviceability limit state 1 (SLS 1). This is reached if $PL1_{y,ms}$ occurs, i.e. dissipaters are subjected to yielding. The dissipaters can be replaced after the event at moderate cost (if external) or they can be left installed. This second option is recommended if the strain deformation is moderate i.e., within 0.5-0.7%.

2. $PL_{1,b}$ defined as serviceability limit state 2 (SLS 2). This is reached if $PL2_{u,ms}$ or $PL1_{dr}$ occurs. In other words, if the dissipaters have to be replaced at the end of the seismic

event (because they are broken) or damage is expected to non-structural elements.

3. PL_2 defined as ultimate limit state (ULS) or controlled damage. This is reached if $PL3_{y,t}$ or $PL2_{dr}$ occurs. In other words, if damage is expected to occur on the main structural elements or the interstorey drift is greater than 2.5%.

4. PL_3 defined as collapse limit state (CLS). This is reached if $PL4_{y,p}$, $PL5_{u,p}$ or $PL3_{dr}$ occurs. In other words, if the system fails or excessive interstorey drift greater than 5% occurs.

5. PL_4 defined as reparability limit state (RLS). This is reached if the residual drift after the earthquake is greater than 0.5%. In other words, if PL_4 is reached the building is not considered repairable due to cost.

FRAGILITY FUNCTIONS FORMULATION

Fragility curves are defined as the probability of overcoming a specific performance level, conditional to an intensity measure, IM, (Shinozuka et al., 2000; Baker, 2015). In earthquake engineering, it is common to assume the lognormal distribution to define the fragility function (Baker, 2015; Porter, 2015), i.e. Equation **??**

$$P(D = d|IM = im; \boldsymbol{\theta}_f) = \Phi\left(\frac{\ln(im/\alpha)}{\beta}\right), \tag{5}$$

where $\Phi(\cdot)$ is the standard normal cumulative distribution function, $\boldsymbol{\theta}_f = [\alpha, \beta]$, α is the median of the fragility function, and β the standard deviation of the logarithm of the IM, in this case the spectral acceleration.

The parameters of the fragility functions are assumed dependent of the post-tensioning level, PT, represented by Equations (6) and(**??**):

$$\alpha(PT) = \mathcal{M}_\alpha(PT), \tag{6}$$

$$\beta(PT) = \mathcal{M}_\beta(PT), \tag{7}$$

where $\mathcal{M}_\alpha(\cdot)$ and $\mathcal{M}_\beta(\cdot)$ are functions describing the relationship between α, β and PT. In this setting, for different levels of PT, the parameter of α and β are first computed using *the same* set of ground motions. Then, the empirical relationships Equations (6)-(7) are derived from tracing the different structural performances for different PT levels. In the following, the ground motion selection is firstly presented; then the derivation of the empirical relationship

(6), (7) is presented, followed by the time dependent fragility including the uncertainty on the PT level.

GROUND MOTIONS SELECTION

The fragility curves were developed by using the multi-stripe method (Baker, 2015). The intensity measure domain was subdivided in "stripes," each one represented by the spectrum given by the New Zealand Standard 1170.5 (2004) for 20, 25, 50, 100, 250, 500, 1000, 2500 years return period, respectively.

For each spectrum (soil category D) representing the seismic hazard, 80 ground motions were selected for the two sites. Ground motions were extracted from the NGA database (Chiou et al., 2008) and scaled with respect to the spectral acceleration in correspondence of the first natural period of the structure (estimated equal to 0.85 s based on the modal analysis). The following conditions were considered during the selection process :

1. the ratio between the spectral acceleration of the original ground motion and the code spectrum in correspondence of the first natural period can not be lower than 0.33 or greater than 3 (New Zealand Standard 1170.5, 2004).
2. the maximum spectral acceleration of the scaled ground motion is not higher than 1.5, which is the maximum spectral acceleration provided by the code.

Both conditions were introduced to avoid:

1. having scaling factors too big or too small which dramatically affect the ground motion intrinsic properties (i.e., a ground motion of low intensity does not have the same frequency content of a ground motion of high intensity (Bradley, 2010));
2. adequately representing the hazard in correspondence of the first natural period as well as the plateu range of periods.

The spectra of the ground motions used in this study are reported in Figure 10 and 11 for low and high seismic zones, respectively.

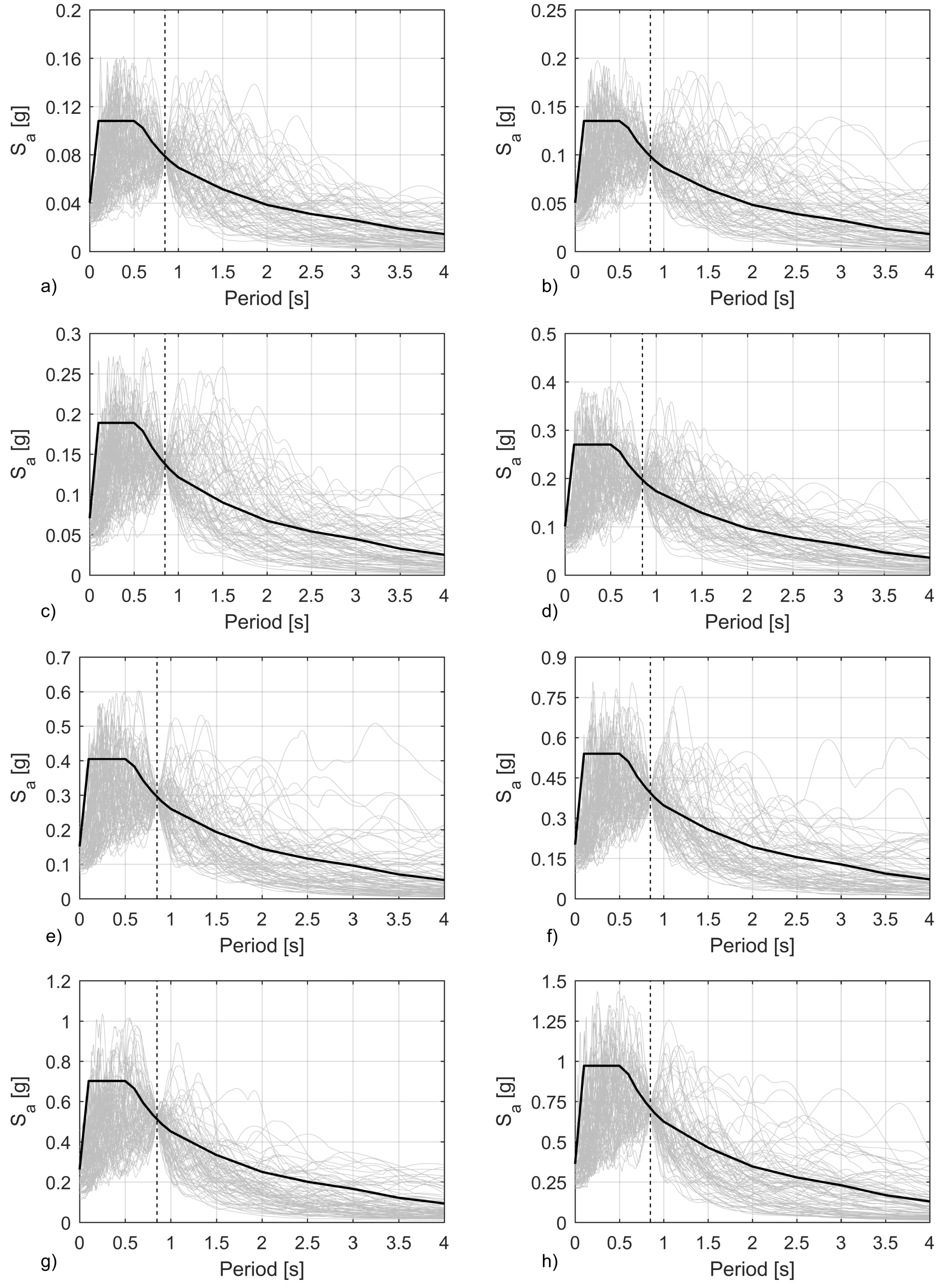

Figure 10. Ground motions spectra for a) 20, b) 25, c) 50, d) 100, e) 250, f) 500, g) 1000 and h) 2500 years return period in low seismic zone. The natural period of the building is also highlighted by a dotted line.

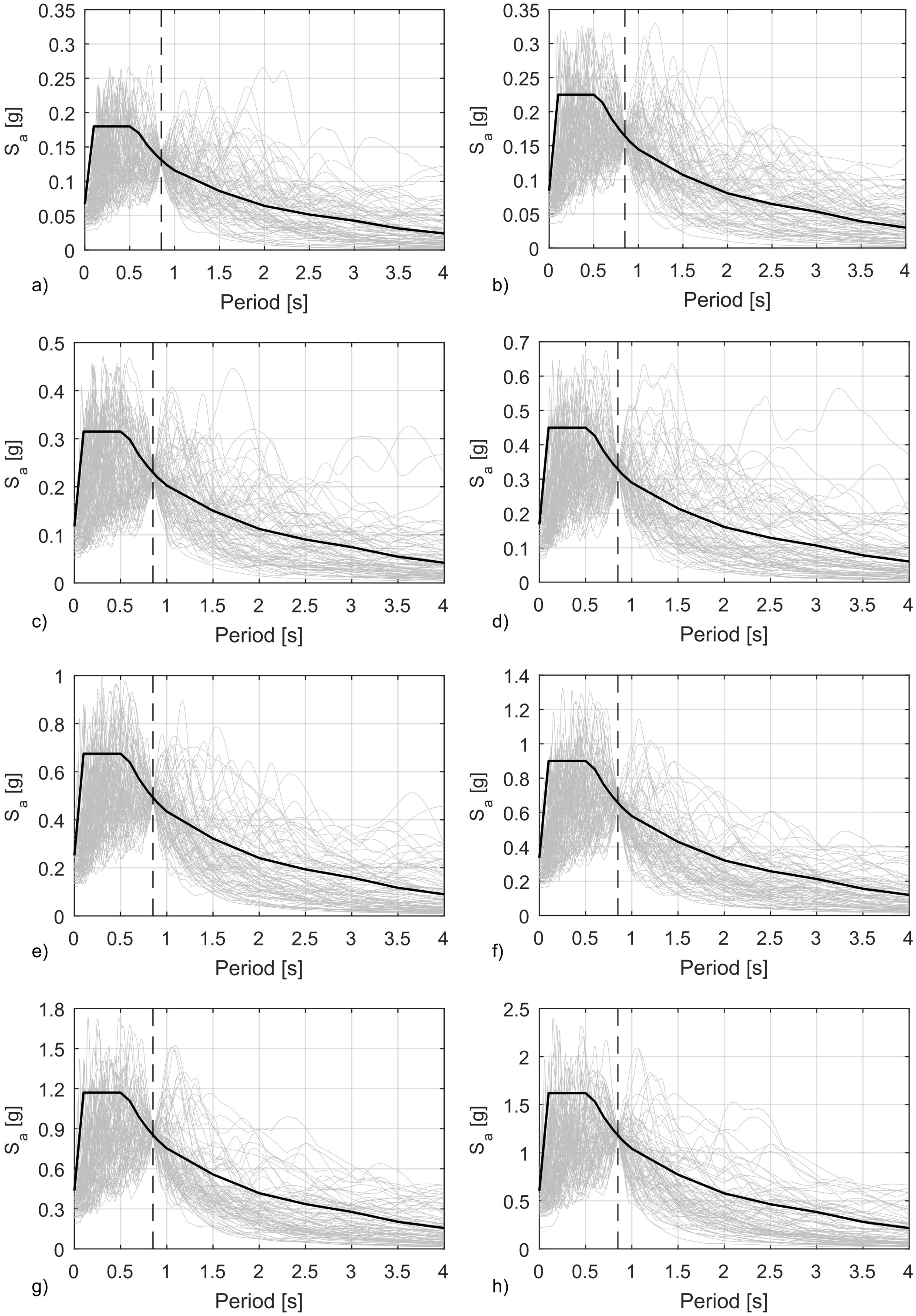

Figure 11. Ground motions spectra for a) 20, b) 25, c) 50, d) 100, e) 250, f) 500, g) 1000 and h) 2500 years return period in high seismic zone. The natural period of the building is also highlighted by a dotted line.

SEISMIC RESPONSE OVER TIME

PARAMETERS OVER TIME

The parameters α and β describing the fragility curves were calculated for 10 levels of post-tensioning loss, i.e., 0%, 5%, 10%, 15%, 20%, 25%, 30%, 35%, 40%, and 45% [b)].

In this study we impose the scaling parameter β for a specific performance level to be constant across the different PT levels, while the location parameter α varies accordingly in a linear model. Imposing a constant β avoids intersection between the fragility curves, which are merely due to "jumps" of β values, due to the classification of EDP points on the onset of a limit state threshold.

Therefore, an average beta β_{avg} is estimated for each curve associated with a specific performance level, and the location parameter, α, is recomputed on the reduced parameter space. This corresponds to the engineering assumption that the reliability of the structural system is uniformly decreasing (across all IM values) with the post tension losses.

The computation therefore involved two iterations and can be summarized as follows:

1. Calculation of α and β as result of Maximum Likewood Estimation (Baker, 2015);
2. Calculation of the average variance β_{avg} as weighted average of the different βs. The weights were calculated normalizing the probability of a specific post-tensioning loss in 50 years.
3. Re-calculation of α by considering β_{avg} instead of β.

The values of β is reported in Figure 12a and 12b for the building without and with supplemental damping, respectively. The continuous line in both figures shows the average value β_{avg}, which is also reported in Table 7.

The values of α are reported in Figures 13a and 13b for the building without and with supplemental damping, respectively. Results were interpolated with the following linear model $\alpha(PT) = \mathcal{M}_\alpha(PT) = a'PT + a_0$, , with values reported in Table 7.

It can be noticed from Figures 13a and 13b that post-tensioning loss has an impact on the fragility curves. The greater the post-tensioning loss, a lower value of α occurs. This means

[b)] The levels were selected based on Figure 6

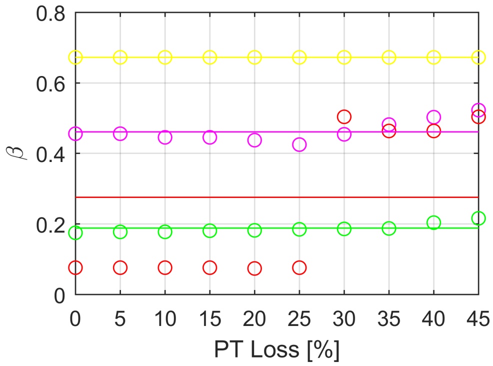

(a) **(b)**

Figure 12. Variance β for the building A) without and B) with supplemental damping.

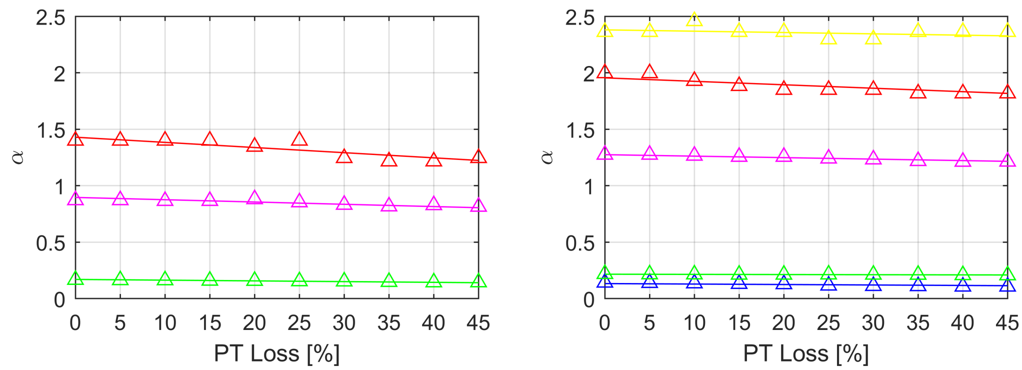

(a) **(b)**

Figure 13. Average α for the building A) without and B) with supplemental damping.

Table 7. Values of β_{avg} and $\alpha = a'x + a_0$, where x is the amount of post-tensioning loss.

	Without dissipaters				**With dissipaters**				
	SLS 2	**ULS**	**CLS**	**RLS**	**SLS 1**	**SLS 2**	**ULS**	**CLS**	**RLS**
β_{avg}	0.188	0.461	0.276	0.672	0.290	0.240	0.311	0.436	0.468
a'	-0.00065	-0.0020	-0.0046	-0.55	-0.00041	-0.00015	-0.0013	-0.0031	-0.0012
a_0	0.170	0.896	1.43	60.7	0.133	0.216	1.27	1.95	2.38

that, generally speaking, for a given intensity measure, the probability of overcoming a specific performance level increases while losses increase.

Note that the values of α for the RLS in the building without additional damping (yellow triangles in Figure 13a) are not present in the graph until the post-tensioning loss reaches 70%. These values are in fact 10 times greater than the CLS, which means the probability of overcoming re-centering is 10 times lower in average than the probability of reaching 6% drift. This was expected because the building does not have dissipaters, and the re-centering ratio is equal to 1 and does not depend on the post-tensioning level. Also, it has to be noted that the α related to re-centering is higher than the α related to collapse. This means that the probability of re-centering is always higher than the probability of collapse.

Considering now the process PT_t of Equation (3), the relationship between(6) and(7) are rewritten as Equations 8 and 9

$$A_t = \mathcal{M}_\alpha(PT_t), = a' PT_t + a_0 \tag{8}$$

$$B_t = \mathcal{M}_\beta(PT_t) = \beta_{avg}, \tag{9}$$

The capital letters A_t and B_t are introduced to highlight the fact that the parameters α, β, for a given time t, are random variables. However, because β is assumed independent on the post-tensioning loss, it is a deterministic value interdependent of time. In Figure 14, the values of α are reported for the building without additional damping. The dotted line represents the response over time of the mean, $\mu_{A_t} = a'\mu_{PT}(t) + a_0$, while the boundaries represent the response considering $\pm 2\sigma_{A_t}$, where $\sigma_{A_t} = a'\sigma_{PT}(t)$. In the same way, the values of A_t for the building with additional dissipaters are reported in Figure 15.

FRAGILITY CURVES

The time variant fragility including the PT uncertainty is given by Equation (**??**):

$$P(D = d | im, \boldsymbol{\Theta}_{f,t} = \boldsymbol{\theta}_f) = \Phi\left(\frac{\ln(im/\alpha)}{\beta} \Big| A_t = \alpha, B_t = \beta_{avg} \right). \tag{10}$$

Then, the mean average fragility over time can be obtained by plugging in the mean value of A_t, i.e.

$$P(D = d | im, \boldsymbol{\Theta}_{f,t} = \bar{\boldsymbol{\theta}}_f) = \Phi\left(\frac{\ln\Big(im/(a'\mu_{PT}(t) + a_0)\Big)}{\beta_{avg}} \right), \tag{11}$$

and the 2STD confidence bounds can be obtain as

$$P(D = d | im, \boldsymbol{\Theta}_{f,t} = \boldsymbol{\theta}_{f,\pm 2\sigma}) = \Phi\left(\frac{\ln\Big(im/\big(a'(\mu_{PT}(t) \pm 2\sigma_{PT}(t)) + a_0\big)\Big)}{\beta_{avg}} \right). \tag{12}$$

Observe that these fragility functions are *marginal* fragility, i.e., they do not include the correlation between different instants of time. It is considered out of the current scope of this study to provide the definition of such time-correlation models mainly because a correlation analysis is

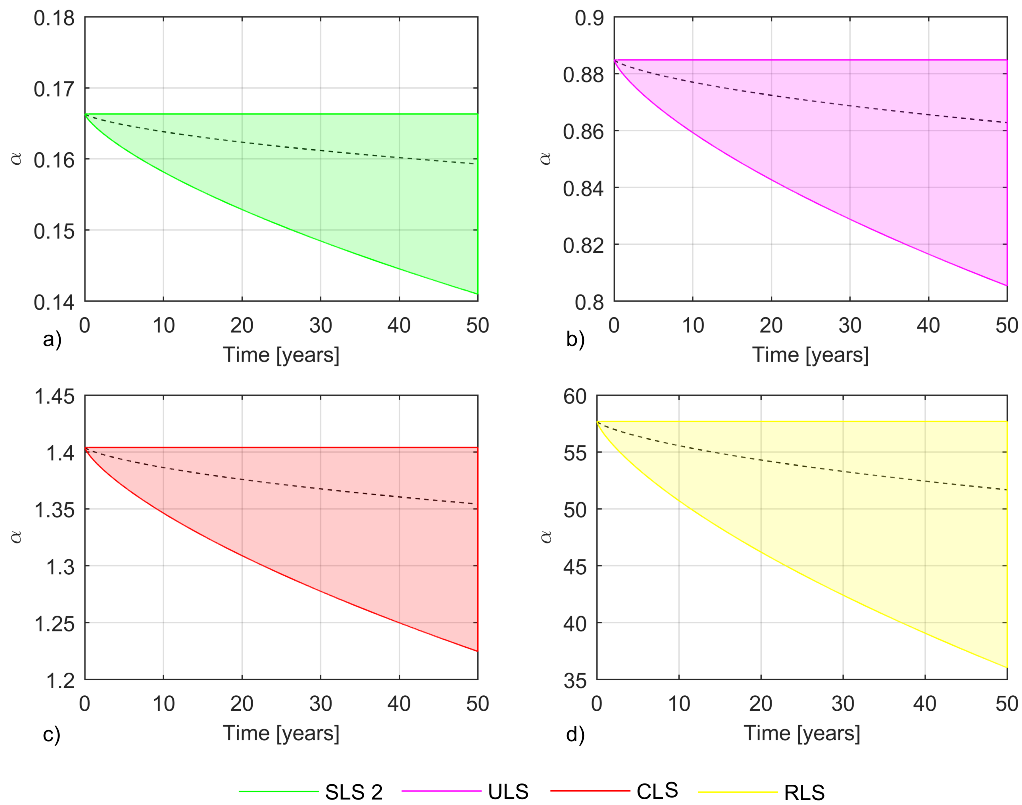

Figure 14. Parameter α over time for each performance level in the building without supplemental damping (black line= mean value μ, boundaries = $\mu \pm 2\sigma$.)

not available. Moreover, no inspections or measurements, which will justify updating the model after information becomes available, are included in the design. In this case a full Gaussian process, which includes a correlation model between different instants of time, can be integrated in the current model. Observe that in this case the current formulations of A_t and B_t play the role of "prior information." Moreover, if only one fragility is desired (instead of a family of fragility) which also includes the PT uncertainty, the following equation can be used

$$P(D = d|im, \boldsymbol{\Theta}_{f,t} = \boldsymbol{\theta}_f) = \int_\alpha \Phi\left(\frac{\ln(im/\alpha)}{\beta}\Big|\alpha, \beta_{avg}\right) f(\alpha|t)d\alpha. \tag{13}$$

The fragility curves at the initial time for the building with dissipaters are reported in Figure 16a. It can be noticed that the building has less than 20% probability to damage the no-structural elements (SLS2) for a seismic event with a return period equal to 25 years, and a considerably small probability (i.e. 0.01%) to damage to the structural elements (ULS) by an event with return period equal to 500 years and less than 16% to exceed a 6% drift (CLS) under an event with a return period equal to 2500 years. Furthermore, for events with a return period lower than 500 years the building shows a probability greater than 99.9% to have residual deformation

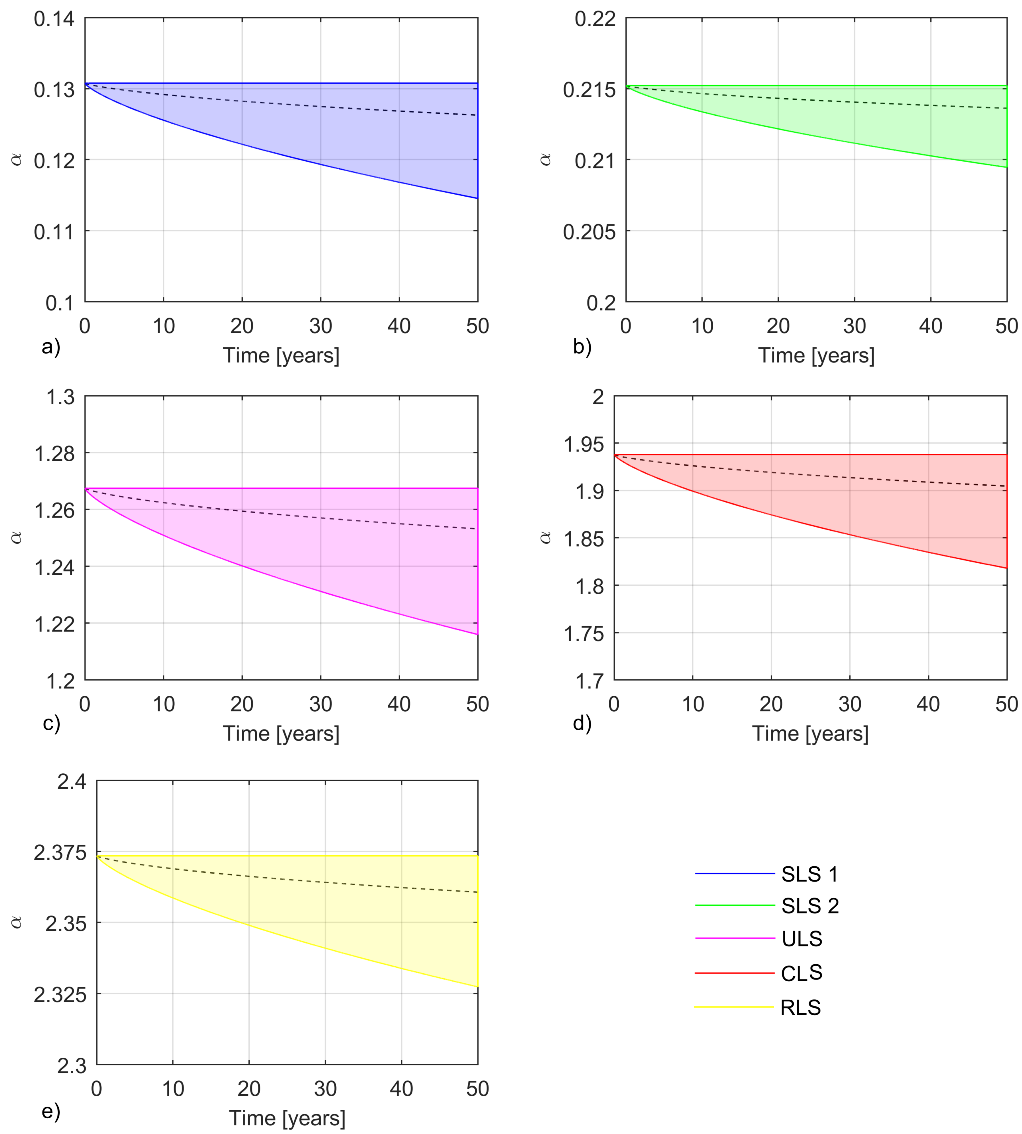

Figure 15. Parameter α over time for each performance level in the building with supplemental damping (black line= mean value μ_{A_t}, boundaries = $\mu_{A_t} \pm 2\sigma_{A_t}$).

smaller than 0.5% drift. Finally, there is 70% probability that the dissipaters are subjected to yielding for an event with a return period equal to 25 years.

Figure 16b reports the family of fragility curves at 50 years. The lower bound is represented by a scenario with post-tensioning loss equal to 45% (i.e., the expected average value minus 2 standard deviations). Results shows that the performance at SLS2, ULS, CLS and RLS is similar to the initial one. However, the probability of yielding the dissipaters increases from 70% to almost 100% for an event with a 25 years return period.

Dissipaters are in fact earlier activated when post-tensioning loss occurs, because the clamp-

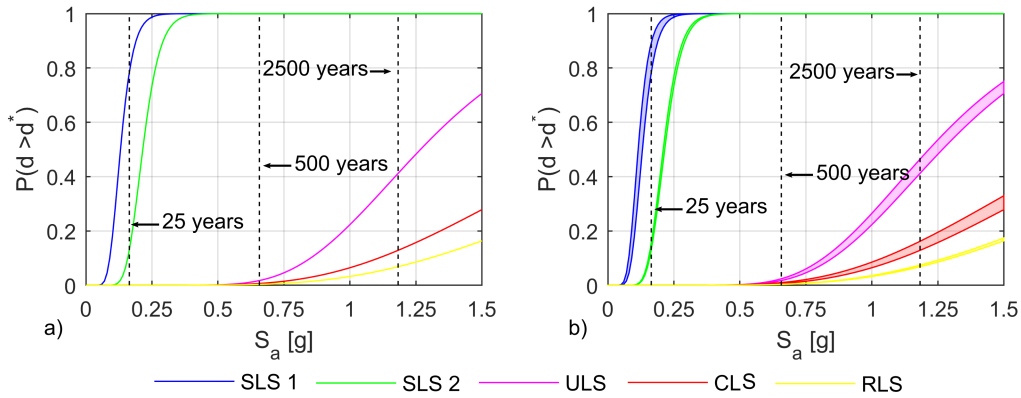

Figure 16. Fragility curves for the building with dissipaters at A) initial time and B) after 50 years.

ing force between the beam and the column is reduced. Therefore, they start dissipating energy at lower level of drift. Because of thisthe interstorey drift does not significantly increase, although the connection capacity is reduced.

However, they are activated more often during the building life, as an event with a lower return period can easily trigger the rocking motion. If dissipaters are external (e.g., in the beam-column joint case), the cost is minor due to the easy access and process. However, if dissipaters are internal (e.g. column-foundation case) the replacement might take more time with a consequently higher cost replacement.

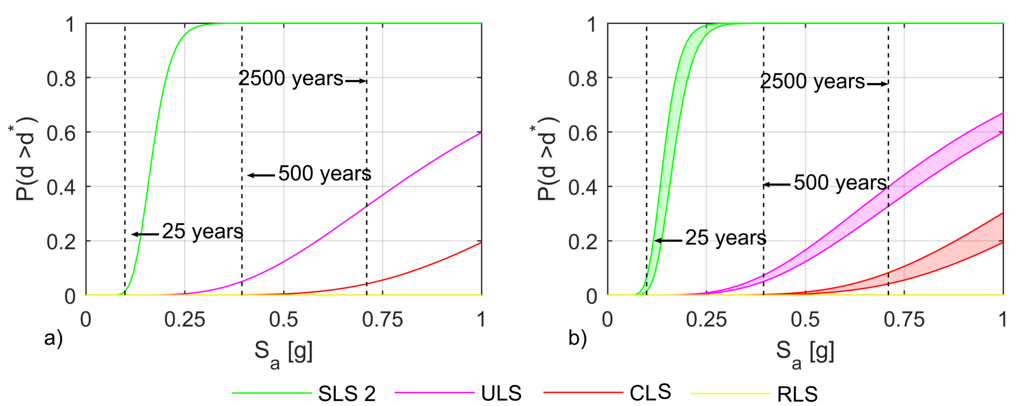

Figure 17. Fragility curves for the building without dissipaters at A) initial time and B) after 50 years.

Figure 17a reports the fragility curves for the building without dissipaters at initial time. It can be noticed the specimen shows approximately 1% probability of damaging the no-structural elements for an event with a 25 years return period; approximately 5% probability of damaging the structural elements for an event with 500 years return period; and less than 5% probability of overcoming 6% drift for an event with a 2500 years return period. Furthermore, the building shows more than 99,9% probability of having a residual interstorey drift lower than 0.5% for all the events with a return period below 2500 years.

Generally speaking, it can be seen from Figure 17b that the area enclosed between the SLS, ULS and CLS curves at initial time and the same curves at 50 years, is greater in respect to the case of the building with additional damping. This means that post-tensioning losses have a greater impact when no dissipaters are provided, and the consequent shift of the fragility curve at 50 years is higher (with respect to the building with additional dissipaters). When looking at design code provisions, the probability of exceeding the SLS, ULS and CLS limit state for specific events with a 25, 500 and 2500 years return period, rises approximately to 7%, 7% and 8% , respectively. This means that the building still shows an acceptable code compliant behavior after 50 years. However, from the pure seismic performance point of view, the greater shift in the fragility curves over time proves that dissipaters mitigate the effect of post-tensioning loss in terms of overall damage.

In terms of re-centring, the building with no dissipaters after 50 years still maintains a probability of exceeding the RLS lower than 0.1% an event with return period lower than 2500 years. This again s due to the fact that, if dissipaters are not provided, the only post-tensioned joint is able to re-center although losses occur.

CONCLUSION

The paper presented a method to evaluate the seismic performance of post-tensioned timber frame buildings through time-dependent fragility curves. The method was then applied to two PresLam frame buildings, which were designed respectively in a high seismic hazard zone (corresponding to a maximum spectral acceleration in correspondence of the plateau equal to 0.9 g for a 500 years return event) and a low seismic hazard zone (corresponding to maximum spectral acceleration in correspondence of the plateau equal to 0.54 g for a 500 years return event).

The building in the high seismic zone was designed by combining unbonded post-tensioned tendons with dissipaters, while the building in the low seismic zone relies only on unbonded post-tensioned tendons.

A set of performance levels was adapted for post-tensioned timber rocking structures. The post-tensioning force over time was predicted by using an available methodology, and the uncertainty in the prediction was also considered by using data monitored on an operative building.

In terms of buildings performance, results show that:

1. the building performance is slightly affected over time. In both cases, the probability of damaging the non-structural elements, damaging the structural elements or collapsing, slightly increases (i.e. 5-10%) after 50 years. Both the structures analyzed (with and without dissipaters) provide a satisfactory performance while considering damage to non-structural elements, damage to structural elements and excessive interstorey drift for events with 25 years, 500 years and 2500 years return period, respectively. If dissipaters are provided, they contribute to reducing the expected increase of interstorey drift due to post-tensioning losses over time.

2. Both buildings show good re-centring capability, i.e., a probability greater than 99.9% of having a residual interstorey drift lower than 0.5% for an event with 500 years return period.

3. The building with additional damping showed an increase of probability (i.e. 30-40%) of yielding the dissipaters over time for low intensity earthquakes. Because the post-tensioning force reduces over time, the rocking motion is activated for lower levels of seismic force. Therefore, dissipaters should be preferably designed (if possible) to be accessible to facilitate the replacement operations and minimize the cost.

This study was focused on middle-rise buildings, i.e., four storey buildings, because they represent the ideal application for post-tensioned timber frame systems. In the case of higher structures, other structural systems are considered more appropriate to the resist lateral loads, such as post-tensioned timber walls .

REFERENCES

1170.0, N., 2002. *New Zealand Standard*. New Zealand.

Baker, J. W., 2015. Efficient analytical fragility function fitting using dynamic structural analysis. *Earthquake Spectra* **31**, 579–599.

Bradley, B. A., 2010. A generalized conditional intensity measure approach and holistic ground-motion selection. *Earthquake Engineering & Structural Dynamics* **39**, 1321–1342.

Brown, A., Lester, J., Pampanin, S., and Pietra, D., 2012. Rebuilding timber navigations offices using a damage-limiting seismic system. In *World Conference on Timber Engineering, Quebec City*.

Chiorino, M., Napoli, P., Mola, F., and Koprna, M., 1984. Structural effects of time-dependent behaviour of concrete. *CEB Bull. No. 142/142 Bis* .

Chiou, B., Darragh, R., Gregor, N., and Silva, W., 2008. NGA project strong-motion database. *Earthquake Spectra* **24**, 23–44.

Christopoulos, C., Filiatrault, A., Uang, C., and Folz, B., 2002. Post-Tensioned Energy Dissipating Connections for Moment Resisting Steel Frames. *Journal of Structural Engineering* **128**, 1111–1120.

Comite Europeen de, N., 2005. *Eurocode 8 - Design of structures for earthquake resistance.* Brussels, Belgium.

Curtain, B., Dekker, D., Chung, S., and Palermo, A., 2012. Design of Carterton Event Centre: An example of innovative collaboration between architecture and timber engineering. In *Proceedings of the 12th World Conference on Timber Engineering WCTE, Auckland, New Zealand*.

Davies, M. and Fragiacomo, M., 2011. Long-term behavior of prestressed LVL members. I: Experimental tests. *Journal of Structural Engineering* **137**, 1553–1561.

Di Cesare, A., Ponzo, F. C., Nigro, D., Pampanin, S., and Smith, T., 2017. Shaking table testing of post-tensioned timber frame building with passive energy dissipation systems. *Bulletin of Earthquake Engineering* **15**, 4475–4498. doi:10.1007/s10518-017-0115-9.

FEMA, P., 2009. 695. Quantification of Building Seismic Performance Factors. *Federal Emergency Management Agency* .

Granello, G., Giorgini, S., Palermo, A., Carradine, D., Pampanin, S., and Finch, R., 2017. Long-Term Behavior of LVL Posttensioned Timber Beams. *Journal of Structural Engineering* **143**, 04017158.

Granello, G., Leyder, C., Palermo, A., Frangi, A., and Pampanin, S., 2018. Design Approach to Predict Post-tensioning Losses in Post-tensioned Timber Frames. *Journal of Structural Engineering* **Accepted**. doi:10.1061/(ASCE)ST.1943-541X.0002101.

Hare, J., Oliver, S., and Galloway, B., 2012. Performance Objectives for Low Damage Seismic Design of Buildings. In *NZSEE conference, Christchurch*.

Holden, T., Devereux, C., Haydon, S., Buchanan, A., and Pampanin, S., 2016. NMIT Arts & Media BuildingInnovative structural design of a three storey post-tensioned timber building. *Case Studies in Structural Engineering* **6**, 76–83.

Kramer, A., Barbosa, A. R., and Sinha, A., 2015. Performance of steel energy dissipators connected to cross-laminated timber wall panels subjected to tension and cyclic loading. *Journal of Structural Engineering* **142**, E4015013.

Leyder, C., Wanninger, F., Frangi, A., and Chatzi, E., 2015. Dynamic response of an innovative hybrid structure in hardwood. *Proceedings of the Institution of Civil Engineers-Construction Materials* **168**, 132–143.

Li, Z., He, M., and Wang, K., 2018. Hysteretic Performance of Self-Centering Glulam Beam-to-Column

Connections. *Journal of Structural Engineering* **144**, 04018031.

Marriott, D., Pampanin, S., and Palermo, A., 2009. Quasi-static and pseudo-dynamic testing of unbonded post-tensioned rocking bridge piers with external replaceable dissipaters. *Earthquake engineering & structural dynamics* **38**, 331–354.

McCormick, J., Aburano, H., Ikenaga, M., and Nakashima, M., 2008. Permissible residual deformation levels for building structures considering both safety and human elements. In *Proceedings of the 14th world conference on earthquake engineering*, pp. 12–17.

Morlier, P., 2004. *Creep in timber structures*, vol. 8. CRC Press.

Moroder, D., Smith, T., Dunbar, A., Pampanin, S., and Buchanan, A., 2018. Seismic testing of post-tensioned Pres-Lam core walls using cross laminated timber. *Engineering Structures* .

New Zealand Standard 1170.1, N., 1993. *New Zealand Standard*. New Zealand.

New Zealand Standard 1170.5, N., 2004. *New Zealand Standard*. New Zealand.

Newcombe, M., Pampanin, S., Buchanan, A., and Palermo, A., 2008. Section analysis and cyclic behavior of post-tensioned jointed ductile connections for multi-story timber buildings. *Journal of Earthquake Engineering* **12**, 83–110.

Palermo, A., 2004. The use of controlled rocking in the seismic design of bridges. *Doctate Thesis, Technical Institute of Milan, Milan* .

Palermo, A., Pampanin, S., Buchanan, A., and Newcombe, M., 2005. Seismic design of multi-storey buildings using laminated veneer lumber (LVL). In *New Zealand Society for Earthquake Engineering Conference*. Wairakei, New Zealand.

Pampanin, S., Palermo, A., and Buchanan, A. H., 2013. Design Guide Australia and New Zealand: Post-Tensioned Timber Buildings. *Expan Design Guides* .

Pampanin, S., Priestley, M. N., and Sritharan, S., 2001. Analytical modelling of the seismic behaviour of precast concrete frames designed with ductile connections. *Journal of Earthquake Engineering* **5**, 329–367.

Ponzo, F. C., Di Cesare, A., Lamarucciola, N., Nigro, D., and Pampanin, S., 2017. Modelling Of Post-tensioned Timber-framed Buildings With Seismic Rocking Mechanism At The Column-foundation Connections. *International Journal of Computational Methods and Experimental Measurements* **5**, 966–978.

Porter, K., 2015. Beginner?s guide to fragility, vulnerability, and risk. *Encyclopedia of Earthquake Engineering* pp. 235–260.

Priestley, M., 2000. Performance based seismic design. *Bulletin of the New Zealand society for earthquake engineering* **33**, 325–346.

Priestley, M., Calvi, G., and Kowalsky, M., 2007. Displacement-based seismic design of structures. *IUSS Press* .

Priestley, N. M. J., 1991. Overview of the PRESSS Research Program. *PCI Journal* **36**, 50–57.

Sarti, F., Palermo, A., and Pampanin, S., 2015. Quasi-static cyclic testing of two-thirds scale unbonded posttensioned rocking dissipative timber walls. *Journal of Structural Engineering* **142**, E4015005.

Sarti, F., Palermo, A., and Pampanin, S., 2016. Fuse-Type External Replaceable Dissipaters: Experimental Program and Numerical Modeling. *Journal of Structural Engineering* **142**, 04016134.

Sarti, F., Palermo, A., Pampanin, S., and Berman, J., 2017a. Determination of the seismic performance factors for posttensioned rocking timber wall systems. *Earthquake Engineering & Structural Dynamics* **46**, 181–200. doi:10.1002/eqe.2784.

Sarti, F., Smith, T., Danzig, I., and Karsh, E., 2017b. Pres-Lam in the US: the seismic design of the Peavy Building at Oregon State University. In *New Zealand Society of Structural Engineers Conference*. Wellington, New Zealand.

Shinozuka, M., Feng, M. Q., Lee, J., and Naganuma, T., 2000. Statistical analysis of fragility curves. *Journal of engineering mechanics* **126**, 1224–1231.

Smith, T., 2014. *Post-tensioned Timber Frames with Supplemental Damping Devices*. PhD Thesis, University of Canterbury, Christchurch, New Zealand.

Valipour, H., Khorsandnia, N., Crews, K., and Palermo, A., 2016. Numerical modelling of timber/timber–concrete composite frames with ductile jointed connection. *Advances in Structural Engineering* **19**, 299–313.

Wanninger, F. and Frangi, A., 2014. Experimental and analytical analysis of a post-tensioned timber connection under gravity loads. *Engineering structures* **70**, 117–129.

Wanninger, F., Frangi, A., and Fragiacomo, M., 2014. Long-Term Behavior of Posttensioned Timber Connections. *Journal of Structural Engineering* pp. DOI: 10.1061/(ASCE)ST.1943–541X.0001121. doi:10.1061/(ASCE)ST.1943-541X.0001121.